Flat Plate Boundary-Layer Studies in a Partially Ionized Gas

RAYMOND C. TSENG* AND L. TALBOT†
Mechanical Engineering Department, University of California, Berkeley

A combined experimental and numerical investigation was conducted on the flat plate boundary-layer flow of a partially ionized gas. Free molecule cylindrical Langmuir probes were used to measure charged particle density, electron temperature and plasma potential distributions in the boundary layer. The ambipolar diffusion flux to the plate surface was determined by an array of flush-mounted surface electrodes. A probe size-study was carried out and an empirical formula was obtained to make correction for the sheath-fringing field effect on ion current collection to small flush probes. Numerical integrations were made of the charged species conservation and electron energy equations in the quasi-neutral region of the boundary layer for a thin plasma sheath. Mechanisms leading to the cooling of the electrons were investigated. Numerical profiles of charged particle density, electron temperature and plasma potential compared favorably with experimental results. Ambipolar diffusion fluxes predicted theoretically agreed very well with the measured flush probe ion saturation current. The validity of employing such a flush-mounted surface electrode in determination of the free stream charged particle density was then established.

Nomenclature

A = probe area
A_0 = quantity appearing in Eq. (2)
C = species concentration; $C \equiv C_+ = C_-(M_+/M_-)$
C_+, C_- = $(N_{i,e}M_{+,-})/\rho$
c,d = constants in Eq. (10)
C_p, C_{p-} = specific heat of atom (ion), electron, respectively; $(\frac{5}{2})(k/M_{+,-})$
D_A = ambipolar diffusion coefficient, $D_A = D_i[1 + (T_e/T_i)]$
D_i, D_e = diffusion coefficients
e = electron charge
E = energy given to electron gas per recombination, in ev
$\bar{f}(\bar{\eta})$ = solution to Blasius equation in $\bar{\eta}$ coordinate
g_s = defined by Eq. (11)
H = reference length
I_i, I_e = ion, electron current to probe
K_a, K_e = thermal conductivities for neutral and electron gases, respectively
Kn = Knudsen number, $\lambda/2r_p$
k = Boltzmann's constant
L = length of flat plate
l = probe length
$\bar{l}$ = Chapman-Rubesin factor; $\rho\mu/\rho_\delta\mu$
M = mass of species
N = species number density
n_i^* = $N_i/(N_i)_\delta$
Pr = Prandtl number; $C_p\mu/K_a$
$\bar{Q}_e$ = electron-ion collisional energy transfer
q = $-\{d(\log C_\delta)/d(\log s)\}$
R = Γ/Γ_{+w}
Re_x = Reynolds number $(\rho_\delta u_\delta x)/\mu_\delta$
r = constant in Eq. (10)
S_A = ambipolar Schmidt number; $\mu/\rho D_A$
s = $\int_0^x \rho_\delta u_\delta \mu_\delta dx$
T, T_e = temperatures of neutral (ion) and electron gases, respectively, °K
T^* = T/T_δ
u,v = velocity components
$\bar{V}_A$ = ambipolar diffusion velocity; $\{-(D_A/C)(\partial C/\partial y)\}$
x = distance from flat plate leading edge
y, y^* = transverse distance, $y^* = y/H$
Z = C/C_δ
α = T_i/T_e
α' = recombination coefficient defined in Eq. (5)
Γ_{+w} = ambipolar diffusion flux to plate surface
$\bar{\eta}$ = transformed boundary-layer coordinate; $\bar{\eta} = \left\{\frac{(\rho_\delta u_\delta)}{[2(\tilde{l}s)^{1/2}]}\right\}\int_0^y\left(\frac{dy}{T^*}\right)$
θ = $T_e/T_{e\delta}$
θ_- = electron temperature in ev
Λ = plasma parameter $\Lambda = 12\pi N_e\lambda_D^3$
λ_D = Debye length, $\lambda_D = (kT/4\pi N_e e^2)^{1/2}$
$\lambda_{i,j}$ = mean free path for species i scattered by species j
μ = viscosity
ν_{ei} = electron-ion collisional frequency
ξ_e = energy transfer due to recombination
ρ = mass density
τ = $T_\delta/T_{e\delta}$
ϕ = potential
ϕ_0 = plasma potential
χ = dimensionless potential difference with respect to plasma potential
$\dot{\omega}$ = volume recombination rate

Subscripts

a,n = atom or neutral
$e,-$ = electron
$i,+$ = ion
f = floating
p = probe
s = sheath
w = wall
λ = one mean free path from surface
δ = boundary-layer edge

Presented as Paper 70-86 at the AIAA 5th Aerospace Sciences Meeting, New York, January 19–21, 1970; submitted March 3, 1970; revision received January 11, 1971. Work supported by the Air Force Office of Scientific Research under AFOSR Grant 538-67.

* Graduate Research Assistant, now Research Staff Member, IBM Research Laboratory, San Jose, California.
† Professor of Mechanical Engineering.

1. Introduction

BOUNDARY-LAYER flow problems associated with a partially ionized gas have received considerable attention in attempts to understand the weakly ionized gaseous environment encountered under many practical conditions. Onboard measurements on re-entry vehicles using a flush-mounted surface electrode have provided a convenient means of obtaining the maximum or boundary-layer edge charged-species density. However, the success of these measurements depends crucially on the success of boundary-layer theory in predicting the charged species properties distributions, and furthermore on how the probe edge effect can be properly taken into account.

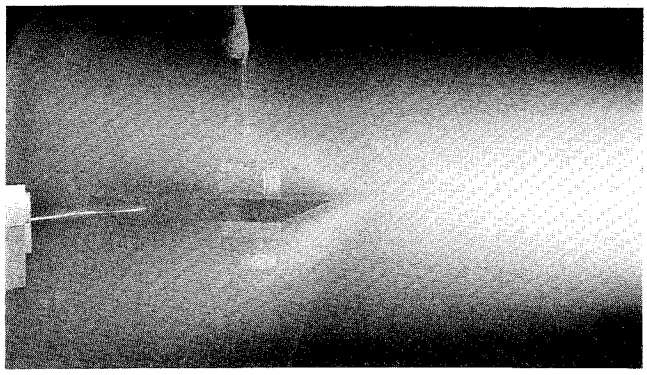

Fig. 1 Nozzle flow over flat plate.

Several analyses[1-3] on the partially ionized boundary-layer flow have been carried out. Most of these analyses are based on the assumption that the electron temperature is either frozen or in equilibrium with that of the heavier species, with the objective of obtaining the current-voltage characteristic of an electrode located on the surface for cases under which the plasma sheath is either collision-dominated or collision-free. Su[4] pointed out that when the body is at floating potential, the structure of the plasma sheath has little effect on the charged species density distribution in the boundary layer. The work of Burke[5] took into account compressibility and electron energy effects and his numerical results showed that the electron temperature decreased only near the edge of a collision dominated sheath.

Experimental investigations on this topic are relatively scarce. Flat plate boundary-layer electron temperature measurements have recently been reported by Brown and Mitchner[6] in a seeded atmospheric argon plasma using a spectroscopic technique. Other flush probe data[7,8] obtained in shock tubes have also been reported. The agreement between experimental data and theoretical analysis is still inconclusive due either to the uncertainty involved in the diagnostic technique or to the approximations contained in the theoretical models.

In the present study, the plasma properties in a flat plate boundary layer were measured by means of free molecule cylindrical probes and flush-mounted electrostatic probes whereas theoretical profiles were obtained through numerical solution of species and electron energy conservation equations taking account of variable transport properties. The main purpose of this paper is therefore to determine to what extent agreement between theory and experiment can be achieved through using a well-understood experimental tool and a realistic theoretical model. The accuracy involved in the determination of the boundary-layer edge ion density from flush probe saturation ion current is also investigated. A size study is presented to demonstrate the sheath-fringing-field effect on ion current collection by a flush probe and an empirical formula is given to make correction for this effect as a function of the ratio of probe radius to sheath thickness.

2. Experimental Flowfield, Flat Plate Model, and Electrostatic Probes

Experiments reported here were performed in a low-density plasma wind tunnel where argon gas was ionized by RF induction at 4 mHz in the stagnation chamber and then expanded through a conical nozzle into the test section. A detailed description of this test facility and its associated instrumentation has been reported elsewhere.[9]

Under test conditions as described in Ref. 10, the plasma flowfield was found to be quite uniform, from both impact pressure and ion density surveys (variations within 10% for 6.5 in. of axial traverse). The reference freestream flow properties are given in Table 1. The model in which the boundary-layer studies were conducted was a flat plate insulated electrically with respect to the wind-tunnel wall and at zero angle of attack. A photograph of the nozzle flow over the plate is shown in Fig. 1.

The flat plate model was water-cooled and constructed of brass with a sharp leading edge (0.005 in.). It had a 1.5-in. groove in the center so that three sets of inserts with different probing arrangements—including static pressure holes, thermocouples, and various flush probes—could be fitted into the groove to become an integral part of the flat plate.

The collection surfaces of the cylindrical Langmuir probes were produced by allowing a length of bare tungsten wire to protrude from a piece of mullite tubing insulation. The probe construction, cleaning, and circuitry have been reported in Ref. 9. Flush-mounted circular electrostatic probes were made of copper rods and insulated from the plate body with BN sleeves. For the charged particle diffusion flux study an array of five $\frac{3}{8}$-in.-diam flush probes situated along the plate centerline were used. Several smaller-sized flush probes made from copper or tungsten wires of the proper cross-sectional area were employed for flush-probe size-studies.

The free molecule cylindrical Langmuir probe used for the boundary-layer surveys had a radius of 6.35×10^{-3} cm and an aspect ratio $l/r_p \simeq 70$. From recent reports by Sonin[11] and Kirchhoff et al.[12] cylindrical probes of this aspect ratio aligned with the flow should produce little end effect and probe theory for an infinite cylinder in stationary plasma should be applicable.

3. Electrostatic Probe Measurements in a Flowing Plasma and Their Applicability to Flat Plate Boundary-Layer Survey

Recent reviews by de Leeuw[13] and Chen[14] gave detailed accounts of electrostatic probe theory and its application. The most accurate collisionless theory published to date is that of Laframboise.[15]

In order that collisionless theory be applied it is necessary that Knudsen numbers based on all relevant mean free paths and the probe dimensions be large. Under our most stringent experimental conditions all Knudsen numbers ($Kn \equiv \lambda/2r_p$) were much larger than unity except $(Kn)_{ii}$, $(Kn)_{ee}$, and $(Kn)_{ei}$, which had minimum values of 0.15, 0.35, and 0.95, respectively. For ion current collection to a cylindrical probe Graf[16] and Sonin[11] have shown that Laframboise's collisionless theory agreed very well with experiments for $(Kn)_{ii}$ down to 0.25 and 0.03. However, for electron temperature measurement it has been found[12] that double probes are less susceptible to collisional effects than single probes. Hence electron temperature was determined from a double probe method which is similar to that of Johnson and Malter[11] but which

Table 1 Nozzle flow conditions

$\dot{m}$	0.45 g/sec
P_{stag}	4.85 torr
P_{chamber}	0.034 torr
Atom/Ion temperature	~850°K
Electron temperature	1620°K
Atom number density	4.1×10^{14} cm^{-3}
Charged particle density	5.5×10^{12} cm^{-3}
Mach number	2.2
Reynolds number/cm	~8
Plate surface temperature	400°K
ν_{ei}	1.33×10^{9} sec^{-1}
λ_D	1.2×10^{-4} cm
λ_{i-n}	3.1×10^{-1} cm
λ_{n-n}	5.0×10^{-1} cm
λ_{e-i}	1.7×10^{-2} cm
λ_{e-n}	1.2×10^{2} cm
λ_{e-e}	5.9×10^{-3} cm
λ_{i-i}	2.3×10^{-3} cm

takes into account the dependence of ion current collection on r_p/λ_D and (T_i/T_e). The improvement was achieved by using Kiel's[18] fitting formula to Laframboise's numerical result. Ion number density was deduced from the ion saturation current using the theory of Laframboise. Details of data reduction and the application of Kiel's fitting formula are described in Ref. 10. The boundary-layer plasma potential distribution was measured indirectly. The cylindrical probe floating potential ϕ_f, with respect to the wind-tunnel wall, was measured and converted to plasma potential according to the collisionless probe theory. Here the dimensionless plasma-floating potential difference $\chi_f \equiv e(\phi_0 - \phi_f)/kT_e$ is also evaluated as a function of r_p/λ_D and T_i/T_e.

The theory for flush mounted electrostatic probes is more complicated and less complete. Its validity in measuring the freestream ionized species properties was not known a priori. But under conditions where the mean free path is much larger than the Debye length and the probe saturation ion current is independent of the bias-potential, this saturation ion current can be used to determine the sheath edge ion density if the electron temperature is known. The sheath edge electron temperature in our case can be determined through extrapolation from the boundary-layer electron temperature profile or by collecting the retarding field electron current through pulsing the flush probe from floating to sheath edge plasma potential, as described in Ref. 10. Since the flush probe ion current saturation could not always be achieved due to the sheath fringing-field effect, a size-study on flush probes was undertaken and served to establish a criterion under which the edge effect starts to become significant.

The ion saturation current collected by flush probes can be used to determine the charged particle number density at the boundary-layer edge by means of boundary-layer theory only if this ion current density agrees with the theoretically predicted ambipolar diffusion flux across the boundary layer. This correspondence can be assessed by comparing the result of a numerical analysis of the charged species conservation equation with experimental measurements using both cylindrical and flush-mounted electrostatic probes.

4. Experimental Results

4.1 Results of Cylindrical Langmuir Probe Measurements in the Boundary Layer

Langmuir probe measurements were made to about 0.1 in. above the flat plate surface. Figure 2 shows boundary layer profiles of electron temperature at two stations behind the leading edge. The boundary-layer edge electron temperature $\theta_{-\delta}$, was essentially constant along the flat plate. The measured electron temperature profile displayed a decrease in θ_- of about 30% of the freestream value towards the plate surface. This is believed to be caused by the cooling effect due to the

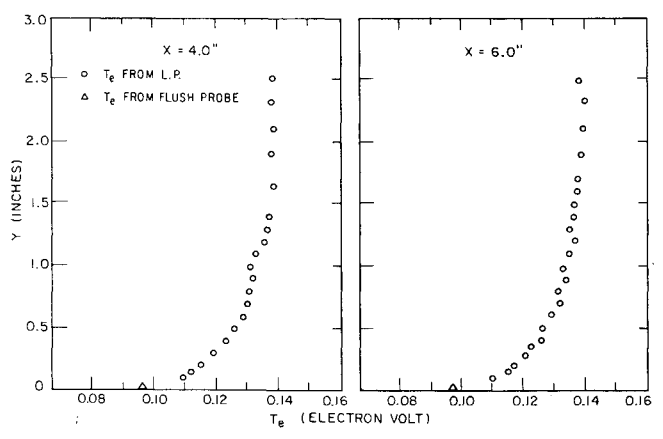

Fig. 2 Boundary-layer electron temperature profiles.

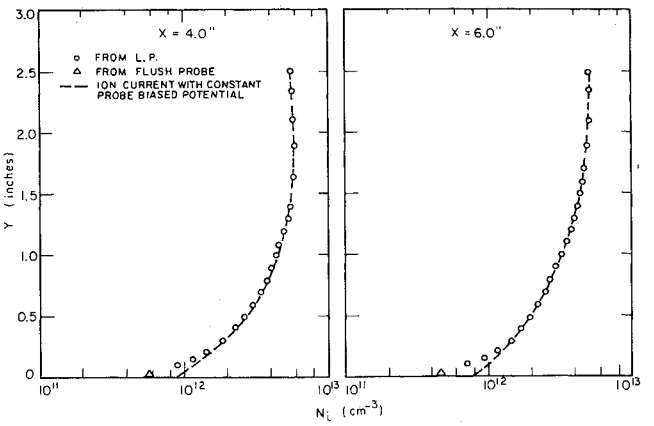

Fig. 3 Boundary-layer charged particle density profiles.

presence of the cooled plate. Although the flat plate at the floating potential collects only a small portion of the electron random flux, it collects the high-energy electrons which carry with them many times the average electron internal energy. Secondly, in an afterglow plasma such as used in our experiment, the electron temperature is significantly influenced by the collisional-radiative 3-body recombination process. In this process, a fraction of the ionization energy is returned to electrons through the so-called "superelastic collisions" and the electron temperature tends to be higher than that of ions and neutrals. This recombination energy transfer shows up as a source term in the electron energy balance as discussed in later sections. The recombination coefficient α' is proportional to the charged particle number density N_i, for θ_- constant. Because the charged-particle density decreased sharply toward the plate surface, the recombination process was then not expected to be adequate in maintaining a constant θ_- throughout the boundary layer. Both of these energy-loss mechanisms contribute to lowering θ_- close to the edge of the plasma sheath over the plate.

The magnitude of the decrease in θ_- across the boundary layer, as shown in Fig. 2 appeared to be similar to the results of Brown and Mitchner.[6] A detailed comparison was not attempted due to the different flow conditions for the two experiments. Our results also exhibit some disagreement with Sonin's[11] θ_- measurements in a stagnation boundary layer in which he found θ_- to be approximately constant all the way to the blunt body surface. The standing normal shock in Sonin's experiment tended to heat the electron gas, as has been shown by Kirchhoff.[19] This heating effect thus balances out part of the cooling effect due to the blunt body so that the depression in θ_-, if any, will be confined to a region extremely close to the surface. Boundary-layer charged particle density profiles obtained by Langmuir probes are shown in Fig. 3. Ion saturation current profiles obtained with constant probe bias are also shown for purposes of comparison. Due to the variation in θ_-, ϕ_0 and r_p/λ_D through the boundary layer, differences between the two profiles can be expected. The ion current profile appeared to over-estimate the ion density near the wall if it was taken to be equivalent to the ion density distribution.

The distribution of floating potential measured relative to the value of ϕ_f at the boundary-layer edge is shown in Fig. 4. The plasma potential distribution calculated according to free molecular probe theory is also included. The potential drop in the ambipolar region is about 0.4 v. This is of the same order as the potential drop through the free fall sheath (estimated to be $5.6\,\theta_{-,s} \simeq 0.6$ v). Negligible charge separation is expected in the ambipolar region because of its much larger length scale compared with the free fall sheath. It is also of interest to note the constancy of the plasma potential from the boundary-layer edge out toward the jet boundary.

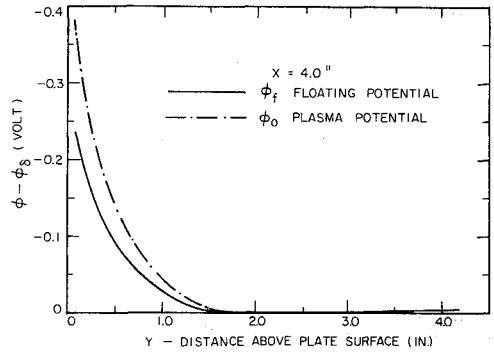

Fig. 4 Boundary-layer floating and plasma potential profiles (x = 4.0 in.).

This demonstrates clearly the fact that no current was flowing when the flat plate was at floating potential.

4.2 Result of Flush Probe Measurements

The ion saturation current collection vs bias potential was essentially constant for $\frac{3}{8}$-in.-diam flush probes. This ion current collection—extrapolated to the floating potential—is presented in Fig. 5 as a function of distance from the leading edge. Since the plate was electrically floating, the ion current to a flush probe at floating potential should represent the ambipolar flux driven to the plate by the combined driving forces due to partial pressure gradient and electric field. Data presented in Fig. 5 indicate that the flush probe ion current along the plate varied nearly as $x^{-1/2}$.

If the ion current collection by flush probe is truly ambipolar in nature, then this ion current can also be obtained by evaluating the ambipolar diffusion flux to the plate surface from the measured ion number density profile and the estimated neutral temperature distribution. As shown later, this ambipolar diffusion flux can be expressed as

$$\Gamma_{+w} = \frac{e}{M_+}\rho D_A \frac{\partial C}{\partial y}\bigg|_\lambda = \frac{e(N_i)_{\max}}{H} D_A \left\{\frac{\partial n_i^*}{\partial y^*} + \frac{n_i^*}{T^*}\frac{\partial T^*}{\partial y^*}\right\}_\lambda \quad (1)$$

where

$$C = N_i M_+/\rho, \quad n_i^* = N_i(N_i)_{\max}, \quad T^* = T/T_\delta, \quad y^* = y/H$$

The quantities $D_A\{\ \}$ on the right-hand side are evaluated at one mean free path away from the plate surface and H is some reference length. Using measured properties in the determination of D_A, n_i^*, and $\partial n_i^*/\partial y^*$, together with an estimate of $(1/T^*)(\partial T^*/\partial y^*)$ from simple boundary-layer theory, Γ_{+w} was calculated as a function of x and is included in Fig. 5. This calculated Γ_{+w} is found to be only about 10% lower than the flush probe measurements and also shows a $x^{-1/2}$ variation. The discrepancy is not serious due to the approximate nature of Eq. (1) in neglecting thermal diffusion, and to the inability of measuring $(\partial n_i^*/\partial y^*)|_\lambda$ accurately from the charged particle density profile.

Because of the relatively close agreement between the flush probe ion current and the calculated diffusion flux Γ_{+w}, the ion current to a flush probe can be used to determine the sheath edge ion number density via

$$(N_i)_{\text{sheath edge}} = [\Gamma_{+w}/(2kT_e/M_+)^{1/2}]/(1 + \alpha)A_0 \quad (2)$$

where A_0 is a function of $\alpha \equiv (T_i/T_e)$ and has been determined in Ref. 10 by making use of a sheath analysis due to Bienkowski.[20] This calculated $(N_i)_{\text{S.E.}}$ has been included in Fig. 3, together with boundary-layer charged species particle measurements obtained by cylindrical probes. It is found that the sheath edge ion number density falls on the line of extrapolation rather well. The T_e used in Eq. (2) is taken as an extrapolation from the boundary-layer T_e profile. In fact, $(T_e)_{\text{S.E.}}$ was also obtained from the retarding field electron current collection by pulsing a $\frac{1}{8}$-in. flush probe from floating potential towards the sheath edge plasma potential. The plot of $\ln I_e$ vs ϕ_p exhibited a straight line for two decades of electron current collection. The flush probe T_e measurements are also shown in Fig. 2 and are consistent with the T_e profiles within the boundary layer.

4.3 Flush Probe Size Study Results

The larger flush probes ($\frac{1}{8}$ and $\frac{3}{8}$ in. diam) operated at negative bias gave essentially identical V-I characteristics and current saturation was approached quickly. For smaller flush probes ion current collection exhibited much stronger dependence on applied potential, as shown in Fig. 6. To demonstrate the sheath-edge effect the current density to smaller flush probes was normalized with respect to the ion current collection at the floating potential as obtained by the $\frac{3}{8}$-in.-diam flush probe and plotted as a function of r_p/l_s in Fig. 7 for several flow conditions. The sheath thickness l_s was calculated with the bias-potential and properties at the sheath edge for a free fall sheath as given in Brown.[21] It is seen that ion current density can increase by a factor of 10 or more if l_s/r_p is rather large.

The excess of ion current density collected by a small flush probe as compared to the ambipolar diffusion flux can be explained as an increase of effective collecting area due to the three-dimensional nature of the plasma sheath near the probe. Considering the sheath to be represented by the curved surface of a spherical segment with height l_s and with its base circle taken to have a radius r_p as shown in Fig. 7, then the ratio of the effective collection area to the actual probe area becomes

$$\bar{R} \equiv (A_{\text{eff}}/A_{\text{probe}}) \simeq 1 + (l_s^2/r_p^2) \quad (3)$$

Equation (3) is also shown in Fig. 7 and appears to agree with experimental data very well for $(l_s/r_p) \geq 1$. For $l_s/r_p < 1$ a better estimate of the effective area can be achieved as described in Ref. 10, which gives

$$\bar{R} \equiv A_{\text{eff}}/A_{\text{probe}} \simeq 1 + (l_s/r_p)^2 + \tfrac{1}{8}(l_s/r_p)[1 - 0.92(l_s/r_p)] \quad (4)$$

5. Numerical Program

A numerical analysis was carried out with the object of examining the depression of electron temperature θ_- toward the surface of the flat plate and the effect of variable transport properties on charged particle density distribution in the boundary layer. Assuming the plasma sheath over the plate surface to be much smaller than any relevant mean free path, which was satisfied under our experimental conditions, profiles of N_i and θ_- were obtained in the quasi-neutral region from numerical solutions to the charged species conservation and electron energy equations. All neutral flow properties were calculated according to the classical theory of Chapman

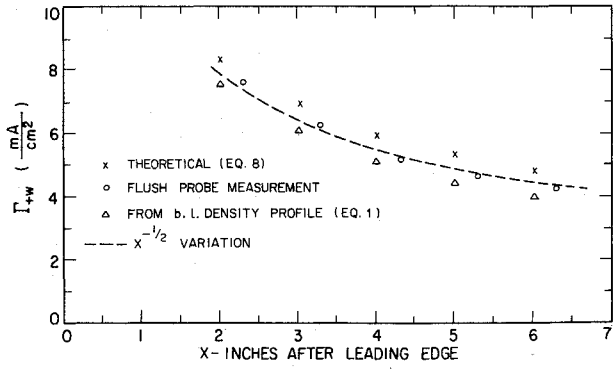

Fig. 5 Comparison of ambipolar diffusion flux values.

and Rubesin.[22] The compressible Blasius velocity profile was assumed to prevail over the plate.

5.1 Species Conservation Equation and Charged Particle Density Profile

For a weakly ionized gas flowing over a flat plate which is at the floating potential, the charged particle diffusion across the boundary layer is essentially ambipolar in nature, and arises as a result of gradients in the partial pressures of ions and electrons and the electric field. Following the formulation of Chung and Blankenship,[2] the charged species conservation equation in the quasi-neutral region of the boundary layer, including the recombination term, can be written as

$$\rho u \frac{\partial C}{\partial x} + \rho v \frac{\partial C}{\partial y} = \frac{\partial}{\partial y}\left\{\rho D_A C\left[\frac{1}{C}\frac{\partial C}{\partial y} + \frac{1}{(1+\alpha^{-1})}\frac{\partial \alpha^{-1}}{\partial y}\right]\right\} + \dot{\omega} M_+ \quad (5)$$

where C is the charged species concentration, D_A is the ambipolar diffusion coefficient, α is the ion-electron temperature ratio, and $\dot{\omega}$ is the volume recombination rate given by Hinnov and Hirschberg[23]: $\dot{\omega} = -(dN_i/dt) = \alpha' N_i^2$, where $\alpha' = 5.6 \times 10^{-27}\,(N_i/\theta_-^{9/2})$ with N_i in cm^{-3} and θ_- in ev.

Equation (5) differs from the more often quoted equation (cf. Brundin[24]) through the inclusion of the additional term $(1+\alpha^{-1})^{-1}(\partial\alpha^{-1}/\partial y)$. However, the inequality $|C^{-1}(\partial C/\partial y)| \gg |[(1+\alpha^{-1})^{-1}(\partial\alpha^{-1}/\partial y)]|$ was always satisfied for our experimental conditions. Hence, for simplicity this extra term is neglected and the simpler equation,

$$\rho u \partial C/\partial y + \rho v \partial C/\partial y = (\partial/\partial y)(\rho D_A \partial C/\partial y) + \dot{\omega} M_+ \quad (6)$$

which was employed by Brundin is also employed here. After applying the usual boundary-layer transformation into $(s,\tilde{\eta})$ coordinates such as used by Chapman and Rubesin,[22] and defining a normalized concentration $Z \equiv C/C_\delta$, we then have

$$(Z'/S_A)' + \tilde{f}Z' = -4qZ[\tfrac{1}{2}\tilde{f}' - Z^2(\rho/\rho_\delta)(\theta_-/\theta_{-\delta})^{-9/2}] \quad (7)$$

in which primes denote differentiation with respect to $\tilde{\eta}$, $S_A \equiv \mu/\rho D_A$ is the ambipolar Schmidt number, and $q \equiv -(\partial \ln C_\delta)/(\partial \ln s)$ is the concentration gradient parameter at the boundary-layer edge due to recombination.

For a constant value of q Eq. (7) can be integrated with calculated profiles of $\tilde{f}$, $\tilde{f}'$, ρ/ρ_δ and measured values of $(\theta_-/\theta_{-\delta})$, subject to the boundary conditions

$$Z(0) = Z_0 \quad \text{and} \quad Z(\infty) = 1, \quad Z'(\infty) = 0 \quad (7a)$$

$Z_0 = 0.02$ is chosen to be consistent with the N_i value at the sheath edge obtained from flush probe data. Numerical integration of Eq. (7) was carried out using a Runge-Kutta scheme with step size $\Delta\tilde{\eta} = 0.1$. The variable ambipolar Schmidt number, S_A, was determined from measured T_e and calculated T_i profiles in the boundary layer. The value of

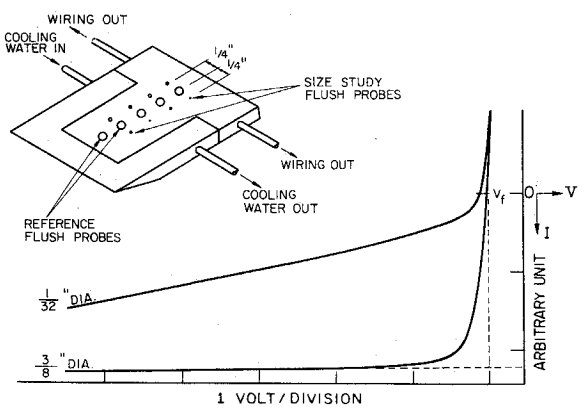

Fig. 6 Size-effect on flush probe characteristics and size-study model schematic.

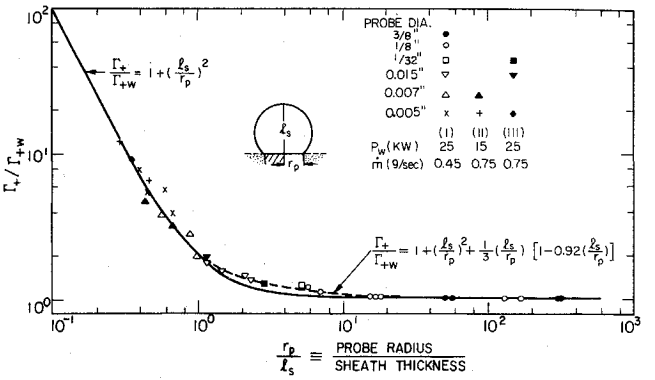

Fig. 7 Size-effect on flush probe ion current collection.

$Z'(0)$ at the sheath edge (or, practically, at the plate surface) was iterated until the desired profile was established for which $Z(\infty) \to 1$ asymptotically.

Figure 8 shows boundary-layer charged particle density profiles for two values of boundary-layer edge concentration gradient parameter q, calculated using the experimental θ_- profile at $x = 4$ inches downstream from the leading edge. The close agreement between these profiles indicates that the effect of volume recombination is manifested mainly in the freestream, where the ion density is the greatest, and thus the boundary-layer profiles normalized by the local freestream ion density show negligible recombination effect. Measured ion density profiles at two stations are plotted in Fig. 9, together with numerically-obtained profiles, neglecting the recombination term. The agreement is good.

The effect of variable ambipolar Schmidt number S_A on the boundary-layer ion density distribution under experimental conditions is also exhibited in Fig. 8. The ion density profiles appeared to be insensitive to whether the S_A variation was determined from the measured θ_- profile or was taken to be a constant value $(S_A)_\delta$. This fact enables us to determine the charged particle density distribution in the boundary layer without exact knowledge of the distribution of electron temperature θ_-. Furthermore, this implies that when the electron energy equation is integrated (as described in Sect. 5.2) the ion density distribution can be assumed known. Otherwise, an iterative procedure has to be used in order to obtain consistent number density and electron temperature profiles.

Under our experimental conditions the neutral mean free path calculated with properties at the plate surface is not negligibly small. The charged particle diffusion flux to the plate surface predicted theoretically should therefore be evaluated one mean free path away from the surface. Ex-

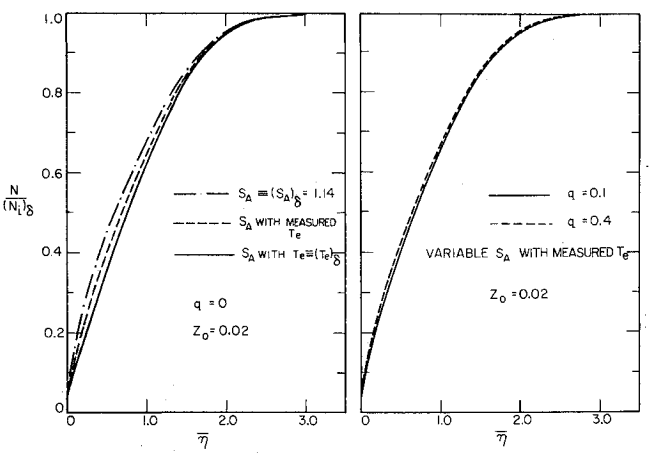

Fig. 8 Theoretical boundary-layer charged particle density profiles ($x = 4.0$ in.).

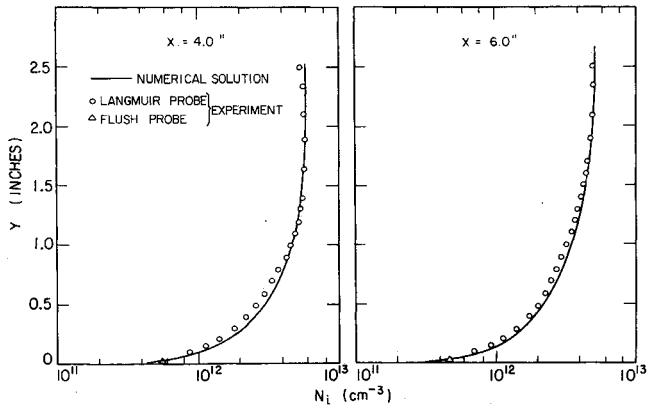

Fig. 9 Comparison of boundary-layer charged particle density profiles.

pressed in boundary-layer variables, we have

$$\Gamma_{+w} = \frac{e}{M_+}\rho D_A\left(\frac{\partial C}{\partial y}\right)\Big|_{y=\lambda} = e(N_i)_\delta \frac{(Re_x)^{1/2}}{x} \times \left\{D_A\left(\frac{\rho}{\rho_\delta}\right)^2 \frac{Z'(\bar\eta)}{2(\bar l)^{1/2}}\right\}_{\bar\eta=\bar\eta_\lambda} \quad (8)$$

where $Re_x \equiv (\rho_\delta u_\delta x)/\mu_\delta$, $\bar l \equiv (\rho\mu/\rho_\delta\mu_\delta)$, and all properties are evaluated at $\bar\eta_\lambda$, the transformed distance for $y = \lambda$.

Using the numerical solution of $Z'(\bar\eta_\lambda)$ for $q \equiv 0$, and the measured value of $(N_i)_\delta$ together with estimated properties D_A, (ρ/ρ_δ), and $\bar l$ at $\bar\eta = \bar\eta_\lambda$, Γ_{+w} can be calculated as a function of x. This result is also presented in Fig. 5, together with experimental measurements using flush probes and free molecule probes. The agreement between measurement and theoretical prediction is excellent (within 10%). This close agreement establishes the fact that the measurement of flush probe diffusion flux Γ_{+w} can be used to determine the charged particle density at the boundary-layer edge through Eq. (8), at least for the present experimental conditions. In general, $Z'(\bar\eta_\lambda)$ is obtained for a fixed value of $Z(0)$ although $Z(0)$ is not known a priori since its determination requires knowledge of $(N_i)_\delta$. This difficulty can be circumvented by starting with an approximate value of $Z(0)$ and obtaining $Z'(\bar\eta_\lambda)$ by integrating Eq. (7) until the boundary conditions are satisfied; on calculating $(N_i)_\delta$ from Eq. (8) and $(N_i)_{S.E.}$ from Eq. (2) using the measured value of Γ_{+w} together with the estimated neutral density ratio, an improved value of $Z(0)$ is obtained. Since the effect of $Z(0)$ on $Z'(\bar\eta_\lambda)$ is quite small, a convergent iterative process can easily be established.

5.2 Electron Energy Equation and Boundary-Layer Electron Temperature and Plasma Potential Profiles

Following the formulation of Dix[25] and with the addition of a recombination energy transfer term, we can write the electron energy conservation equation within the quasi-neutral region in terms of customary boundary-layer notation,

$$\rho C_{-}C_{p,-}\{u\partial T_e/\partial x + (v + \bar V_A)\partial T_e/\partial y\} - (\partial/\partial y)(K_e\partial T_e/\partial y) = \bar Q_{ei} + \xi_e \quad (9)$$

where C_{p-} is the specific heat for the electron gas, $\bar V_A$ is the ambipolar diffusion velocity, K_e is the electron thermal conductivity given by Spitzer,[26] ξ_e is the energy transfer of recombination, and $\bar Q_{ei}$ is the electron-ion collisional energy transfer. The electron-atom collisional energy transfer is neglected because it is negligible relative to $\bar Q_{ei}$. The latter collisional energy transfer is given by

$$\bar Q_{ei} = -4N_e(M_-/M_+)\nu_{ei}k(T_e - T)$$

where the ion and atom temperature is assumed equal and ν_{ei} is the electron-ion collision frequency as given in Holt and Haskell[27]

$$\nu_{ei} = (2.63N_e \ln\Lambda/T_e^{3/2})\ \text{sec}^{-1}$$

where N_e is in cm^{-3}, T_e is in °K and $\ln\Lambda$ is taken to be approximately 6.0. The energy transfer term can be expressed as

$$\xi_e = -(dN_e/dt)E = \alpha' N_e^2 E$$

where α' is given by Hinnov and Hirschberg[23] and E is the energy in ev given to the electron gas per recombination.

In deriving Eq. (9), conduction and diffusion terms for the x direction are assumed to be small compared with those for the y direction. The electron energy transfer term involving the ambipolar electric field has been neglected due to its negligible contribution as compared to the conduction and collision terms.

Transforming into boundary-layer coordinates with $\theta \equiv T_e/T_{e\delta}$, and after substituting the various quantities defined above and using the following relations for the thermal conductivities, $K_a \sim T^{3/4}$, $K_e \sim T_e^{5/2}$, we obtain

$$\frac{\partial^2\theta}{\partial\bar\eta^2} = -\frac{5}{2}\frac{(\partial\theta/\partial\bar\eta)^2}{\theta} + \left\{\frac{0.75}{T^*}\left(\frac{\partial T^*}{\partial\bar\eta}\right) - c\left[\bar f Z + \frac{1}{S_A}\left(\frac{\partial Z}{\partial\bar\eta}\right)\right]\frac{T^{*3/4}}{\theta^{5/2}}\right\} \times \left(\frac{\partial\theta}{\partial\bar\eta}\right) + d\left(\frac{X}{L}\right)\left\{\frac{Z^2(\theta - \tau T^*)}{T^{*1/4}\theta^4} - r\frac{Z^3}{T^{*5/4}\theta^7}\right\} \quad (10)$$

where

$$c = Pr(CK_a/K_e)_\delta$$

$$d = 4Pr(K_a/K_e)_\delta\, 8.9 \times 10^{-20}(N_{e\delta}^2/T_{e\delta}^{1/2})/(\rho_\delta u_\delta C_p T_{e\delta}/L) = 4 \cdot 8.9 \times 10^{-20}(N_{e\delta}^2/T_{e\delta}^{1/2})L^2/K_{e\delta}T_{e\delta}Re_L$$

$\tau = (T_a/T_e)_\delta$ is the neutral-electron temperature ratio at the boundary-layer edge, and $r = E[0.2(N_{e\delta}/T_{e\delta}^4)]$ is the ratio of the recombination term to the collisional energy transfer term.

The boundary conditions for Eq. (10) are specified at the outer edges of the free-fall sheath and of the boundary layer. Following the treatment of Dix,[25] a thin transitional layer is postulated to exist between the sheath and the quasi-neutral region. Assuming electron energy loss and potential drop across this thin transitional layer to be negligible, the net electron energy flux crossing the outer edge of the transitional layer is equated to the net energy flux crossing the edge of the free fall sheath. As shown in Ref. 10, this yields a relationship between $\partial\theta/\partial\bar\eta$ and θ at the sheath edge in the form

$$(\partial\theta/\partial\bar\eta)_s = g_s\Gamma_{+w}\theta_s^{-3/2} \quad (11)$$

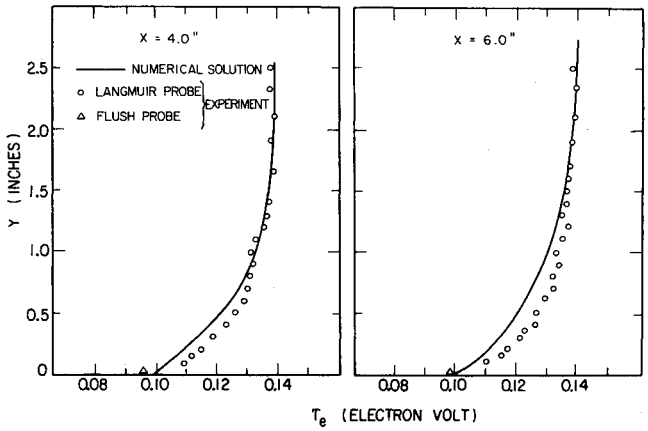

Fig. 10 Comparison of boundary-layer electron temperature profiles.

where

$$g_s = 2(\chi_f - \tfrac{1}{2})\bar{l}^{1/2}(\rho_\delta/\rho_s)(x/Re_x^{1/2})(k/e/K_{e\delta})$$

with χ_f being the dimensionless potential drop across the sheath and Γ_{+w} the ambipolar diffusion flux to the plate surface which is also equal to the electron flux when the probe is at floating potential.

At the boundary-layer edge we have

$$\theta \to 1 \quad \text{and} \quad \partial\theta/\partial\bar{\eta} \to 0 \quad \text{as} \quad \bar{\eta} \to \infty \tag{12}$$

From Eq. (10) this condition also requires that we have collisional-recombination energy balance at the boundary-layer edge. Further, it also determines the amount of energy E given back to the electron gas due to recombination in order to achieve collision-recombination energy balance and from Eq. (10) for $\eta \to \infty$ we obtain

$$E = (1 - \tau)\ 5.0T_{e\delta}^4/(N_e)_\delta \text{ ev} \tag{13}$$

where $T_{e\delta}$ is in °K and $(N_e)_\delta$ is in cm^{-3}. This choice of E enables the numerically integrated boundary-layer profile of T_e to approach $(T_e)_\delta$ asymptotically. The values of E calculated from Eq. (13) using $(N_e)_\delta$, $(T_e)_\delta$ under our experimental conditions range from 1.55 to 2.20 ev per recombination, which are somewhat higher than values of E from a theoretical curve given by Chen[28] for an optically thin plasma. This fact suggests the possibility that some trapping of resonance radiation may have been present. For a more realistic analysis E should be chosen as variable across the boundary layer, but a constant value which is evaluated at the boundary-layer edge seems adequate for our purpose.

Taking x as a parameter, Eq. (10) was integrated using a four point Runge-Kutta scheme with previously determined T_i and N_i profiles across the boundary layer taken as known functions. The numerical results for T_e are shown in Fig. 10, together with Langmuir probe T_e measurements in the quasi-neutral region for two stations behind the leading edge. The calculated and measured T_e profiles agree within 10%. The flush probe θ_- measurements identify quite well the magnitude of the T_e drop close to the surface as predicted by the numerical solutions.

In the derivation of the species conservation equation, Eq. (6), the ambipolar electric field is related to the concentration gradient by

$$\partial(\phi/\theta_{-\delta})/\partial y = (\theta/C)\partial C/\partial y \tag{14a}$$

The potential drop can then be obtained from integration of this ambipolar electric field,

$$\frac{\phi_\delta - \phi(\bar{\eta})}{\theta_{-\delta}} = \int_{\bar{\eta}}^{\delta} \frac{\partial(\phi/\theta_{-\delta})}{\partial\bar{\eta}} d\bar{\eta} = \int_{\bar{\eta}}^{\delta} \frac{\theta}{\partial\bar{\eta}} \frac{\partial \ln Z}{\partial\bar{\eta}} d\bar{\eta} \tag{14b}$$

The plasma potential distribution for $x = 4$ inches calculated by means of Eq. (14b) is plotted in Fig. 11 together with boundary-layer potential measurements made with a floating single probe. Both profiles exhibit the correct trend of potential variation. The single probe measurements exhibit a slightly more rapid potential drop near the plate surface. This discrepancy is believed to be due partly to the small departure between the actual profiles and the theoretically calculated profiles of electron temperature θ and charged species concentration Z in the boundary layer. In fact, the use of measured values of $(\theta_-/\theta_{-\delta})$ and $(N_i/N_{i\delta})$, together with the calculated T/T_δ profile in Eq. (14b) results in improved agreement with the experiment. This agreement would be even better if the thermoelectric effect term $\alpha\nabla\theta_-$ due to the variation of electron temperature in the boundary layer were taken into account of the right hand side of Eq. (14a).

6. Conclusions

An experimental investigation has been undertaken using free molecule cylindrical probes and flush mounted electrostatic probes as primary diagnostic tools for an ionized flat plate boundary layer. A comparison with numerical solutions to boundary-layer species and electron energy conservation equations has shown that the charged species properties predicted by classical boundary-layer theory taking into account variable transport properties agree rather well with the experimental results under moderately low Reynolds number conditions.

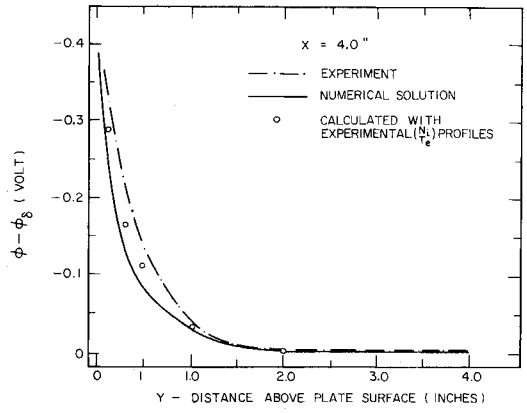

Fig. 11 Comparison of boundary-layer plasma potential profiles (x = 4.0 in.).

Electron temperatures were found to decrease about 30% from the freestream to the plate surface. Mechanisms responsible for cooling the electron gas in the boundary layer were identified as the loss of high-energy electrons to the surface and the inadequacy of recombination energy transfer to the free electrons close to the plate surface because of locally low charged particle densities. Hence electron temperatures measured by flush probes do not correspond to $(\theta_-)_\delta$ at the boundary-layer edge.

The ambipolar diffusion flux to the electrically floating plate was found to be proportional to $x^{-1/2}$ as predicted by the classical boundary layer theory. Flush probe ion saturation current measurements can be used to predict $(N_i)_\delta$ via boundary-layer theory with good accuracy.

The sheath fringing-field effect on ion current collection to a negatively biased flush probe has been established experimentally from results of flush probe size studies. For $l_s/r_p <$ 0.1, the fringing field effect will be less than 5%.

References

[1] Talbot, L., "Theory of the Stagnation Point Langmuir Probe," *The Physics of Fluids*, Vol. 3, No. 2, March–April 1960, pp. 289–298.

[2] Chung, P. M. and Blankenship, V. D., "Theory of Double Electrostatic Probes Comprised of Two Parallel Plates," *AIAA Journal*, Vol. 4, No. 3, March 1966, pp. 442–450.

[3] Lam, S. H., "A General Theory for the Flow of Weakly Ionized Gases," *AIAA Journal*, Vol. 2, No. 2, Feb. 1964, pp. 256–262.

[4] Su, C. H., "Compressible Plasma Flow over a Biased Body," *AIAA Journal*, Vol. 3, No. 5, May 1965, pp. 842–848.

[5] Burke, A. F., "Theoretical Studies of Continuum, Weakly Ionized Gas Flow Including Compressibility and Electron Energy Effects," AN-2101-Y-1, 1967, Cornell Aeronautical Lab., Buffalo, N. Y.

[6] Brown, R. T. and Mitchner, M., "Measurements in a Two-Temperature Plasma Boundary Layer," AIAA Paper 69-692, San Francisco, Calif., 1969.

[7] Bredfelt, H. R., Scharfman, W. E., Guthart, H., and Morita, T., "Boundary Layer Ion Density Profiles as Measured by Electrostatic Probes," TR 33, 1966, Stanford Research Inst., Menlo Park, Calif.

[8] Burke, A. F., "Electrical Currents to a Flat Plate in Supersonic Ionized Flows," AIAA Paper 68-166, New York, 1968.

[9] Peterson, E. W. and Talbot, L., "Langmuir Probe Response in a Turbulent Plasma," *AIAA Journal*, Vol. 8, No. 8, Aug. 1970, pp. 1391–1398.

[10] Tseng, R. C., "Flat Plate Boundary Layer Studies in a Partially Ionized Gas," AS-69-14, 1969, Univ. of California, Berkeley, Calif.
[11] Sonin, A. A., "Free Molecule Langmuir Probe and its Use in Flowfield Studies," *AIAA Journal*, Vol. 4, No. 9, Sept. 1966, pp. 1588–1596.
[12] Kirchhoff, R. H., Peterson, E. W., and Talbot, L., "An Experimental Study of the Cylindrical Langmuir Probe Response in the Transition Regime," AS-69-13, 1969, Univ. of California, Berkeley, Calif.
[13] deLeeuw, J. H., "Electrostatic Plasma Probes," *Physico-Chemical Diagnostics of Plasmas*, T. P. Anderson et al., eds., Northwestern University Press, Evanston, Ill., 1963, pp. 65–95.
[14] Chen, F. F., "Electrostatic Probes," *Plasma Diagnostic Techniques*, R. H. Huddlestone and S. L. Leonard, eds., Academic Press, New York, 1965, pp. 113–119.
[15] Laframboise, J. G., "Theory of Spherical and Cylindrical Langmuir Probes in a Collisionless, Maxwellian Plasma at Rest," 100, 1966, Institute for Aerospace Studies, Toronto.
[16] Graf, K. A., "The Determination of Spatially Non-uniform Electron Density Distribution," 108, 1965, Institute for Aerospace Studies, Toronto.
[17] Johnson, E. O. and Malter, L., "A Floating Double Probe Method for Measurement in Gas Discharges," *Physical Review*, Vol. 80, No. 1, Oct. 1, 1950, pp. 58–68.
[18] Kiel, R. E., "Electrostatic Probe Theory for Free Molecular Cylinders," *AIAA Journal*, Vol. 6, No. 4, April 1968, pp. 708–712.
[19] Kirchhoff, R. H., "An Experimental Investigation of the Shock Structure in a Partially Ionized Gas," AS-69-8, 1969, Univ. of California, Berkeley, Calif.
[20] Bienkowski, G. K., "Electrostatic Sheath in a Weakly Ionized Gas," *The Physics of Fluids*, Vol. 10, No. 2, Feb. 1967, pp. 381–390.
[21] Brown, S. C., *Introduction to Electrical Discharges in Gases*, 1st ed., Wiley, New York, 1966.
[22] Chapman, D. R. and Rubesin, M. W., "Temperature and Velocity Profiles in the Compressible Boundary Layer with Arbitrary Distribution of Surface Temperature," *Journal of the Aeronautical Sciences*, Vol. 16, No. 9, Sept. 1949, pp. 547–565.
[23] Hinnov, E. and Hirschberg, J. G., "Electron-Ion Recombination in Dense Plasmas," *Physical Review*, Vol. 125, No. 3, Feb. 1, 1962, pp. 795–801.
[24] Brundin, C. L., "The Application of Langmuir Probe Technique to Flowing Ionized Gases," AS-64-9, 1964, Univ. of California, Berkeley, Calif.
[25] Dix, D. M., "Energy Transfer in a Partially Ionized, Two-Temperature Gas," ATN-64(9232)-1, 1964, Aerospace Corp., El Segundo, Calif.
[26] Spitzer, L., *Physics of Fully Ionized Gases*, 2nd ed., Interscience, New York, 1962, pp. 143–145.
[27] Holt, E. H. and Haskell, R. E., *Foundations of Plasma Dynamics*, 1st ed., Macmillan, New York, 1965, p. 270.
[28] Chen, C. J., "Partition of Recombination Energy in the Decaying Rare Gas Plasmas," *Physical Review*, Vol. 163, No. 1, Nov. 5, 1967, pp. 1–7.

JULY 1971 AIAA JOURNAL VOL. 9, NO. 7

Cathode Region of a Quasi-Steady MPD Arcjet

P. J. TURCHI* AND R. G. JAHN†
Princeton University, Princeton, N.J.

An MPD discharge is examined near the cathode of a 2.5 Mw, quasi-steady, self-field arcjet. High-speed photography shows a concentration of arc luminosity in the cathode region, while detailed measurements with electric and magnetic field probes indicate that 85% of the total arc power is deposited within one base diameter of the cathode surface. Ion energies are shown to be proportional to the voltage drop in the cathode region even though current conduction is accomplished primarily by electrons in a tensor manner. It is found that a high-speed plasma flow is delivered to the cathode, where it is converted into a useful exhaust jet in a thin, high-density layer at the cathode surface. Local measurements of electron temperature and estimates of electron density, made within the discharge and exhaust jet using a twin Langmuir probe technique, indicate a nearly uniform electron temperature of about 1.5 ev throughout the quasi-steady arcjet flow.

I. Introduction

OUR purpose here is to understand the physical processes involved near the cathode of an MPD arcjet. Interest in such processes derives from a desire to achieve logical guidelines for the design of an optimum electric thruster of this type for space applications. We shall be particularly concerned with the mechanics of current conduction and plasma acceleration in the vicinity of the cathode, and the transfer of electrical energy to the plasma in this region.

Presented as Paper 70-1094 at the AIAA 8th Electric Propulsion Conference, Stanford, Calif., August 31–September 2, 1970; received November 9, 1970; revision received February 22, 1971. Work supported by NASA Grant NGL 31-001-005.

* Graduate Student; now Plasma Physicist, Air Force Weapons Laboratory, Kirtland Ari Force Base, N. Mex.
† Professor of Aerospace Sciences, AMS Department, Guggenheim Aerospace Propulsion Laboratories. Associate Fellow AIAA.

II. Experimental Program

Experiments inside steady MPD arcjets are ordinarily prohibited by the small volume of the arc chamber and the violence of arc operation. Understanding of MPD processes has thus been limited to inferences made from various terminal properties such as total voltage, current, thrust, etc., supplemented by optical measurements of arc-luminosity distribution, and species existence and temperature. We seek to improve this situation by a series of detailed measurements within a high power, large radius, quasi-steady arcjet.

Experimental Facility

By operating an arcjet with a short pulse of high current, we are able to avoid the experimental difficulties of poor interior access and instant probe destruction. Higher currents allow us to scale the arc-chamber dimensions to maintain the intensity of MPD operation in a larger volume. Thus, for a